Journal of Non-Crystalline Solids 369 (2013) 44–54

Contents lists available at SciVerse ScienceDirect

Journal of Non-Crystalline Solids

journal homepage: www.elsevier.com/ locate/ jnoncrysol

Solid-state NMR examination of alteration layers on nuclear waste glasses

Kelly A. Murphy [a], Nancy M. Washton [b], Joseph V. Ryan [c], Carlo G. Pantano [d], Karl T. Mueller [a,b,*]

[a] Department of Chemistry, The Pennsylvania State University, 104 Chemistry Building, University Park, PA 16802, USA
[b] William R. Wiley Environmental Molecular Sciences Laboratory, Pacific Northwest National Laboratory, P.O. Box 999, Richland, WA 99352, USA
[c] Radiological Materials & Technology Development Group, Pacific Northwest National Laboratory, P.O. Box 999, Richland, WA 99352, USA
[d] Department of Materials Science & Engineering, The Pennsylvania State University, N317 Millennium Science Complex, University Park 16802, USA

ARTICLE INFO

Article history:
Received 4 February 2013
Received in revised form 19 March 2013
Available online 16 April 2013

Keywords:
Solid-state NMR;
Alteration layers;
Nuclear waste glass;
AFCI;
Corrosion

ABSTRACT

Solid-state nuclear magnetic resonance (NMR) is a powerful tool for probing the role and significance of alteration layers in determining the kinetics for the corrosion of nuclear waste glass. NMR methods are used to probe the chemical structure of the alteration layers to elucidate information about their chemical complexity, leading to increased insight into the mechanism of altered layer formation. Two glass compositions were examined in this study: a glass preliminarily designed for nuclear waste immobilization (called AFCI) and a simplified version of this AFCI glass (which we call SA1R). Powdered glasses with controlled and known particle sizes were corroded in ASTM type I water at 90 °C for periods of one and five months with a glass surface-area to solution-volume ratio of 100,000 m^{-1}. ^{1}H–^{29}Si cross-polarization Carr-Purcell-Meiboom-Gill (CP-CPMG) magic angle spinning (MAS) NMR, ^{1}H–^{27}Al CP-MAS NMR, ^{1}H–^{11}B CP-MAS NMR, and ^{1}H–^{23}Na CP-MAS NMR experiments provided isolated structural information about the alteration layers, which differ in structure from that of the pristine glass. Both glasses studied here develop alteration layers composed primarily of $^{[IV]}Si$ species. Aluminum is also retained in the alteration layers, perhaps facilitated by the observed increase in coordination from $^{[IV]}Al$ to $^{[VI]}Al$, which correlates with a loss of charge balancing cations. The mechanism of increasing coordination appears to occur through an unstable $^{[V]}Al$ intermediate. ^{1}H–^{11}B CP-MAS NMR observations indicated a retention of boron in the hydrated glass layers, which has not been characterized by previous work. For the AFCI glass, secondary phase formation begins during the corrosion times considered here, and these new phases are detected within the alteration layers. We identify new phases (termed as precursor phases) as crystalline sodium metasilicates. An important finding is that simple glass compositions, while providing general trends about the formation of alteration layers, do not account for all of the various reaction products that occur in the corrosion of more complex nuclear waste glass compositions.

1. Introduction

Current storage solutions for radioactive waste storage include immobilization of the radioactive species in a borosilicate glass matrix by vitrification [1]. It is expected that long-term environmental exposure of vitreous waste forms will lead to changes in glass structure, especially when water breaches the burial sites and permeates any secondary barrier material [1]. Ultimately, the interactions of water and glass will influence the stability of the waste form. Therefore, systematic structural characterizations of altered glasses, specifically their surfaces, are needed to provide insight into the mechanism of glass corrosion and the viability of specific glass compositions for use in the long-term stabilization of radionuclides. In this study, the term "alteration layers" is defined to include any material that has been changed from the pristine glass (with respect to either the composition or structure) due to the exposure to water, including the formation of secondary phases either from structural rearrangement or precipitation from solution.

Several physical mechanisms contribute to corrosion in varying extents with time. For convenience, the general behavior of glasses in static (non-refreshing) solutions can be broken into a series of steps that progress with time and ion concentration in solution [1–6]. The *initial* release of ions is due mainly to interdiffusion, with the contribution of hydrolysis processes rapidly increasing. During interdiffusion, water enters the glass matrix and soluble species such as sodium and boron are released to the surrounding solution. Hydrolysis is characterized by water attack of network forming bonds including those within Si–O–Si linkages. The total hydrolysis of network bonds generates orthosilicic acid or other similar species at higher pH values (H_4SiO_4, $H_3SiO_4^-$, $HSiO_4^{2-}$), which are released to solution (diffusion and affinity). As the reaction proceeds, the release of ions slows and alteration layers begin to build on the surface. The alteration layers can be comprised of multiple sub-layers depending on the conditions and length of corrosion; a simplistic view is presented in Fig. 1. Here we define

* Corresponding author at: Department of Chemistry, The Pennsylvania State University, 104 Chemistry Building, University Park, PA 16802, USA. Tel.: +1 814 863 8674; fax: +1 814 865 2927.
E-mail address: karl.mueller@pnnl.gov (K.T. Mueller).

0022-3093/$ – see front matter © 2013 Elsevier B.V. All rights reserved.
http://dx.doi.org/10.1016/j.jnoncrysol.2013.03.021

three regions involved in corrosion: the pristine glass, the hydrated glass layer, and the gel layer (see further discussion below) (Fig. 1). In particular, some of the decrease in silica release is due to the restructuring or reprecipitation of silica species as a silica rich gel layer. As corrosion proceeds, the rate of release generally stabilizes and eventually reaches a slow constant value known as the residual rate that persists, often indefinitely. In some cases, however, a renewal of relatively rapid alteration can occur after long times due either to the *in situ* reorganization or precipitation of secondary phases at the gel–water interface.

The low dissolution rate reduction observed in the residual rate regime has been attributed alternately to the increased levels of aqueous silicon species and formation of a transport-limiting surface alteration layer(s). This alteration not only reduces the intrinsic reactivity of the surface, but also decreases the transport kinetics associated with the water-glass interdiffusion reactions. Grambow and Muller [10] proposed a first order rate equation to describe glass dissolution kinetics based on the observation that orthosilicic acid concentration controls the reaction rate [1,7–11]. The rate equation was derived from the work of Aagaard and Helgeson [12] on mineral dissolution, which show similar kinetic trends [1,12,13]. Evidence also suggests that one or more of the alteration layer(s) formed during glass corrosion can act as a diffusion barrier to slow important interdiffusion reactions (Fig. 1) [1]. The exact nature of the transport-limiting alteration layer(s) is/are also debated [4,14–20]. As depicted in Fig. 1, the largest alteration layer is primarily a nanoporous silica gel generated by network hydrolysis and local condensation [19–23]. The retention or *in situ* precipitation of components in the gel is dictated by solubility, thermodynamics, and kinetic considerations [1,24]. We define the interfacial region between the gel and pristine glass as the hydrated glass. This layer consists of similar components to those in the pristine glass (albeit in different proportions depending on loss of mobile species), but significantly greater hydrogen content [14]. Eventually, components in the hydrated glass layer will either be lost to solution or participate in gel layer formation. The GRAAL model, which is under investigation as a theory for the prediction of nuclear waste glass behavior, uses a mathematically defined layer to restrict the transport of components that control glass dissolution [1,4,25]. The layer is proposed to be a hydrated glass and the critical species is postulated to be water, but this detail is not important to the current GRAAL model. Although Gin et al. [4] successfully identified a one-micron thick hydrated glass layer by nanoscale-secondary-ion mass spectrometry (NanoSIMS), its role in glass corrosion is still somewhat unclear. Crystalline secondary phases have also been observed to form usually on the surface of the porous gel layer at the gel–water interface or within the gel itself [4,16,18–20,26].

Due to the rather complex coupled nature of leaching, alteration layer formation, and dissolution, it has been difficult to determine the rate-limiting step(s) and mechanism(s) that result in the observed glass behaviors at all times. Previous work has focused on the composition and growth rate of the alteration layers, but their chemical structure and dynamics have not been well characterized [4,14,15,27,28]. Nuclear magnetic resonance (NMR) can provide detailed information about atomistic connectivity (bonding) or proximity (spatial localization), which may yield mechanistic information about the formation of alteration layers through a mapping of solid-state structural details to time-dependent behaviors. The simplest solid-state NMR experiments, the so-called Bloch decay measurements, are combined with magic angle spinning (MAS) to provide *bulk measurements* since structural information is averaged across the entire glass specimen (including both altered and pristine regions). Therefore, these simple experiments cannot isolate information about surface structures, which are much more important for understanding reaction mechanisms. Fortunately, intrinsic properties of the reacting glasses can be exploited to selectively probe the alteration layers.

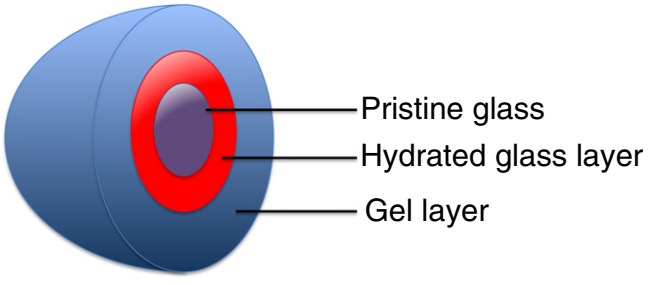

Fig. 1. The alteration layers are subdivided into two layers: the hydrated glass layer and the gel layer. The hydrated glass layer is the interface between the gel layer and pristine glass. The gel layer is in direct contact with the solution phase.

Cross-polarization (CP) magic angle spinning NMR (CP-MAS NMR) utilizes the distance-dependent dipolar coupling between nuclei to transfer spin polarization from one species (such as ^{1}H) to another (e.g., ^{29}Si, ^{11}B, ^{23}Na, or ^{27}Al). In the studies presented here, ^{1}H nuclei act as the source of magnetization in the CP experiments, but notably they are not present in detectable amounts in our pristine glass systems. Within the alteration layers, however, hydrogen atoms are found in the form of hydroxyls, loosely bound water, or other related species. Thus, the transfer of polarization from the hydrogen atoms to constituent nuclei within the alteration layers yields specific and selective information directly corresponding to the structures found within the alteration layers.

Two glass compositions were chosen for this study. The first (AFCI) is a 28-component glass that was developed at the Pacific Northwest National Laboratory (PNNL) for reprocessing waste products (Table 1). The second (SA1R) is a simplified version of AFCI, containing only 8 oxide components (Table 1). Due to its simpler composition, studies of SA1R are expected to more precisely isolate the individual role of specific components during the initial corrosion regime, where silicic acid and silica gel are the primary reaction products. Comparisons between the two glasses could also provide enhanced details about the mechanism of alteration layer(s) formation. Furthermore, the ability to make generalizations about complex glass structure from simple compositions will be addressed, which has been absent from previous work [24,29,30]. We will also make comparative comments to the known behavior of another glass composition, SON68, which is the non-radioactive version of the French R7T7 glass. Although it was formulated for different waste products than the AFCI glass, previous studies of SON68 can provide a guide for data interpretation since it has been extensively investigated [1,31].

2. Experimental procedures

2.1. Glass melting

AFCI glass was prepared from reagent grade materials in 500 g batches at PNNL. The glass was melted for 1 h at 1250 °C in a platinum–rhodium crucible. The glass melt was quenched (by pouring onto a stainless steel plate), crushed, and then re-melted for an additional hour. Detailed melting conditions and characterization of the glass can be found in [32]. Notably, the AFCI samples originally contained a proportion of fine particles generated from crushing (<20 μm) that were not removed by rinsing techniques (Section 2.2). SA1R glass was prepared at the Pennsylvania State University using reagent-grade materials: Min-U-Sil SiO_2 from U.S. Silica, H_3BO_3 from Macron Chemicals, Na_2CO_3 from Alfa Aesar, $CaCO_3$ from Fisher Scientific, Li_2CO_3 from Mallinckrodt Incorporated, Al_2O_3 from Alfa Aesar, ZrO_2 from Potters Industries, and La_2O_3 from Cerac Inc. Batch material was melted in a platinum crucible with a lid at 1275 °C for 1 h and then quench poured on a stainless steel plate. The glass was subsequently crushed in a tungsten carbide ball mill and re-melted for an additional

hour at 1275 °C before final quenching. We attempted to remove fine particles, generated from crushing, from the SA1R glass as described below.

2.2. Corrosion experiments

Corrosion experiments were conducted under similar conditions outlined in the ASTM Standard C1285 Product Consistency Test [33]. A brief description of those conditions will be presented here and further details can be found in the ASTM Standard [33]. Glass was crushed into powder and sieved to less than 32 μm diameter particle size for AFCI and 20–32 μm particle size for SA1R. Fine particles generated from crushing were removed from SA1R powder through rinses with ASTM Type I water and ethanol. The surface areas for these powders were determined by Brunauer–Emmett–Teller surface area measurements (Table 2, Section 2.3.1). Powder was reacted in PFTA digestion bottles at 90 °C for various time periods with ASTM type I water and an original surface area to volume (S/V) ratio of 100,000 m^{-1}. Solution pH was not adjusted and therefore allowed to drift for the one month and five month exposure time period. An "accelerated" (AL) SA1R sample was corroded for one week using an initial solution pH of 11.5, adjusted with 5 M KOH. At the conclusion of the desired period, the powder samples were separated from the solution by vacuum filtration. Solution pH values were measured and the solution compositions determined by ICP-AES or ICP-MS (Section 2.3.2). Powdered samples were allowed to equilibrate under atmospheric conditions overnight before NMR analyses.

2.3. Characterization techniques

2.3.1. BET measurements

BET measurements were conducted either on a Micrometrics ASAP 2020 or Gemini 2370 instrument with Kr adsorption to determine the specific surface area of the glasses.

Table 1
Glass compositions determined by ICP-AES and ICP-MS via HNO_3/HF and sodium peroxide digestion techniques.

Oxide	AFCI (wt.%)	SA1R (wt.%)
Ag_2O	0.04	–
Al_2O_3	9.38	10.40
B_2O_3	9.65	9.88
BaO	0.85	–
CaO	5.00	5.72
CdO	0.04	–
Ce_2O_3	1.19	–
Cs_2O	1.10	–
Eu_2O_3	0.07	–
Gd_2O_3	0.06	–
La_2O_3	0.61	4.88
Li_2O	4.50	5.22
MoO_3	1.50	–
Na_2O	7.00	6.95
Nd_2O_3	2.01	–
PdO	0.01	–
Pr_2O_3	0.56	–
Rb_2O	0.16	–
RhO_2	0.03	–
RuO_2	0.08	–
SeO_2	0.03	–
SiO_2	53.67	55.90
Sm_2O_3	0.41	–
SnO_2	0.03	–
SrO	0.38	–
TeO_2	0.25	–
Y_2O_3	0.24	–
ZrO_2	1.15	0.80
Total	100	99.75

Table 2
Brunauer–Emmett–Teller surface areas measured by Kr adsorption.

Sample	Surface area (m^2/g)
SA1R	0.3
AFCI	3.0

2.3.2. ICP-AES and ICP-MS measurements

Inductively-coupled plasma concentration measurements were conducted utilizing either a Perkin-Elmer Optima 5300UV instrument for atomic emission detection (ICP-AES) or a Thermo Fisher Scientific Xseries 2 instrument for mass spectrometric detection (ICP-MS). Glass compositions were determined via hydrofluoric acid and sodium peroxide digestions (Table 1). If possible, solution analyses were conducted in triplicate under acidification.

2.4. Solid-state NMR analysis

2.4.1. ^{27}Al MAS NMR

^{27}Al MAS NMR experiments were conducted at a magnetic field strength of 11.7 T utilizing a Varian/Chemagnetics Infinity 500 instrument interfaced to a 3.2 mm double resonance NMR probe. The corresponding transmitter frequency was 130.253 MHz. Experiments for all samples utilized a spinning rate of 17 kHz and multiple transients were acquired to obtain sufficient signal-to-noise ratios. A 1 s pulse delay was used between radiofrequency pulses of 2.50 μs, which provided a tip angle of π/20 for the central transition resonance of ^{27}Al nuclei. The chemical shifts were referenced to an external standard sample of aqueous (1.0 M) $AlCl_3$.

2.4.2. ^{11}B MAS NMR

^{11}B MAS NMR experiments were conducted at a magnetic field strength of 19.96 T utilizing an Agilent 850 MHz NMR spectrometer interfaced to a 3.2 mm quadruple resonance NMR probe at the William R. Wiley Environmental Molecular Sciences Laboratory (EMSL) at Pacific Northwest National Laboratory (PNNL). The corresponding transmitter frequency was 272.6322 MHz. Experiments for all samples utilized a spinning rate of 20 kHz and 800 transients were acquired. A radiofrequency pulse of 0.45 μs, corresponding to a tip angle of π/20 for the central transition, and a pulse delay of 4 s were used. The chemical shifts were referenced to a solid boric acid standard with a chemical shift of 19.6 ppm.

2.4.3. ^{29}Si MAS NMR

^{29}Si MAS NMR experiments were conducted at a magnetic field strength of 9.4 T on a home-built spectrometer with a Tecmag pulse programmer interfaced to a 4.0 mm double resonance NMR probe at a ^{29}Si transmitter frequency of 79.463 MHz. Experimental conditions included the acquisition of a total of 1500 transients, a π/2 pulse of 4.00 μs, a pulse delay of 60 s, and a spinning speed of 11 kHz. Chemical shifts were referenced to tetramethylsilane via a secondary standard of solid tetrakis(trimethylsilyl)silane.

2.4.4. ^{23}Na MAS NMR

^{23}Na MAS NMR experiments on AFCI were conducted at a magnetic field strength of 17.6 T utilizing a Varian 750 MHz instrument at EMSL and a 3.2 mm double resonance NMR probe. A radiofrequency pulse of 2.00 μs was used at a resonance frequency of 211.650 MHz. All samples had a spinning rate of 18 kHz and 40,000 transients were acquired. A pulse delay of 1 s was utilized between scans. The chemical shifts were referenced using solid NaCl, which was assigned a chemical shift of 7.1 ppm with respect to aqueous (1.0 M) NaCl.

^{23}Na MAS NMR experiments on SA1R were conducted at a magnetic field strength of 11.7 T utilizing a Varian/Chemagnetics Infinity 500 instrument interfaced to a 3.2 mm double resonance NMR probe.

A radiofrequency pulse of 5.00 μs was used at a resonance frequency of 132.1089 MHz. All samples had a spinning rate of 17 kHz and 10,000 transients were acquired. A pulse delay of 2 s was utilized between scans. The chemical shifts were referenced to NaCl with a chemical shift of 7.1 ppm with respect to aqueous (1.0 M) NaCl.

2.4.5. ^{1}H–^{27}Al CP-MAS NMR

^{1}H–^{27}Al CP-MAS experiments on AFCI samples were conducted at a magnetic field strength of 18.79 T utilizing an Agilent 800 MHz NMR spectrometer with a 4 mm Doty double resonance probe at the EMSL facility. The corresponding transmitter frequencies were 799.5478 MHz for ^{1}H and 208.3413 MHz for ^{27}Al. A π/2 pulse of 4.00 μs was applied to ^{1}H nuclei with a pulse delay of 5 s. Spinning speeds of 8 kHz were used to collect 100,000 transients with high power ^{1}H decoupling. The contact time was optimized for a maximum signal at 500 μs using a Catapal B standard. All chemical shifts were referenced to an aqueous (1.0 M) $AlCl_3$ standard.

^{1}H–^{27}Al CP-MAS experiments on SA1R samples were conducted on a Bruker AVANCE 7.05 T magnet interfaced to a 4 mm double-resonance probe. The resonance frequencies for ^{1}H and ^{27}Al were 300.4296 and 78.2819 MHz, respectively. A π/2 pulse of 4.78 μs was applied to ^{1}H nuclei with a pulse delay of 2 s. Spinning speeds of 10 kHz were used to collect 80,000 transients with high power ^{1}H decoupling. CP-match conditions were established using Catapal B as a standard. A contact time of 400 μs was utilized. All chemical shifts were referenced to an aqueous (1.0 M) $AlCl_3$ standard.

2.4.6. ^{1}H–^{11}B CP-MAS NMR

^{1}H–^{11}B CP-MAS experiments were conducted on a Varian 19.96 T magnet with a 3.2 mm quadruple resonance probe at the EMSL facility. The corresponding transmitter frequencies were 849.7399 MHz for ^{1}H and 272.6322 MHz for ^{11}B. A π/2 pulse of 4.50 μs was applied to ^{1}H nuclei with a pulse delay of 2 s. Spinning speeds of 20 kHz were used to collect 30,000–50,000 transients with high power ^{1}H decoupling. A contact time of 1325 μs was established for the boric acid standard, which was also used for chemical shift referencing.

2.4.7. ^{1}H–^{29}Si CP-CPMG MAS NMR

^{1}H–^{29}Si CP-Carr Purcell Meiboom Gill (CPMG) MAS experiments for AFCI were conducted on a Varian 14.1 T magnet with a 3.2 mm double resonance probe at the EMSL facility. The corresponding transmitter frequencies were 599.8692 MHz for ^{1}H and 119.1751 MHz for ^{29}Si. A π/2 pulse of 2.90 μs was applied to ^{1}H nuclei with a pulse delay of 5 s. Spinning speeds of 8 kHz were used to collect 44,800 transients with high power ^{1}H decoupling. A contact time of 5000 μs was established for the silica gel standard. In order to generate the CPMG sequence, 10 loops were used with $\tau_1 = \tau_2 = 1000$ μs. Other parameters included a dwell time of 0.2 μs, a total acquisition time of 81.92 ms, and a total of 40,960 points.

^{1}H–^{29}Si CP-CPMG MAS experiments for SA1R were conducted on a Varian 19.96 T magnet with a 4.0 mm triple resonance probe at the EMSL facility. The corresponding transmitter frequencies were 849.7399 MHz for ^{1}H and 168.8176 MHz for ^{29}Si. Pulse parameters varied slightly for each sample, but the typical values are reported here. A π/2 pulse of 3.40 μs was applied to ^{1}H nuclei with a pulse delay of 5 s. Spinning speeds of 8 or 10 kHz were used to collect 28,000 transients with high power ^{1}H decoupling. A contact time of 5300 μs was established for the silica gel standard. In order to generate the CPMG sequence, 20 loops were used with $\tau_1 = \tau_2 = 800$ μs. Other parameters included a dwell time of 0.2 μs, a total acquisition time of 102.4 ms, and a total of 25,600 points.

2.4.8. ^{1}H–^{23}Na CP-MAS NMR

^{1}H–^{23}Na CP-MAS experiments were conducted on a Varian 14.1 T magnet interfaced to a 3.2 mm double-resonance probe. The resonance frequencies for ^{1}H and ^{23}Na were 599.9071 and 158.6859 MHz, respectively. A π/2 pulse of 3.00 or 3.50 μs was applied to ^{1}H nuclei with a pulse delay of 10 s. Spinning speeds of 15 kHz were used to collect 20,000–80,000 transients with high power ^{1}H decoupling. A contact time of 1900 or 3500 μs was established for the $Na_2CO_3 \cdot H_2O$ standard. All chemical shifts were referenced to a NaCl standard.

All NMR data were processed with NUTS NMR processing software (Acorn, Inc.).

3. Results and discussion

3.1. Normalized loss

The presence of a higher proportion of fine particles (not removed by rinsing techniques) on the AFCI samples resulted in significantly different aqueous corrosion behaviors relative to SA1R (Fig. 2). Comparisons of relative release of ions are reported as normalized loss values, which take into account the surface area to volume ratio and glass composition:

$$NL\left(g/m^2\right) = \frac{C_s}{X\frac{S}{V}}, \tag{1}$$

where NL is the normalized loss, C_s is the solution concentration, X is the mass fraction of the species, and S/V is the initial powder surface area to volume ratio. In these calculations, BET surface area was used since we could not calculate a geometric surface area for AFCI. The rapid dissolution of fine particles on AFCI resulted in lower normalized loss values. Ebert et al. [34] indicated that AFCI enters the residual rate regime after ~50 days of corrosion; however, the experiments were conducted with a surface to volume ratio of 15,000 m^{-1}. Therefore, the differences in calculation methods make direct comparisons difficult. Our conditions utilized a smaller particle size fraction and higher S/V ratio, resulting in lower normalized loss values. The limited kinetic

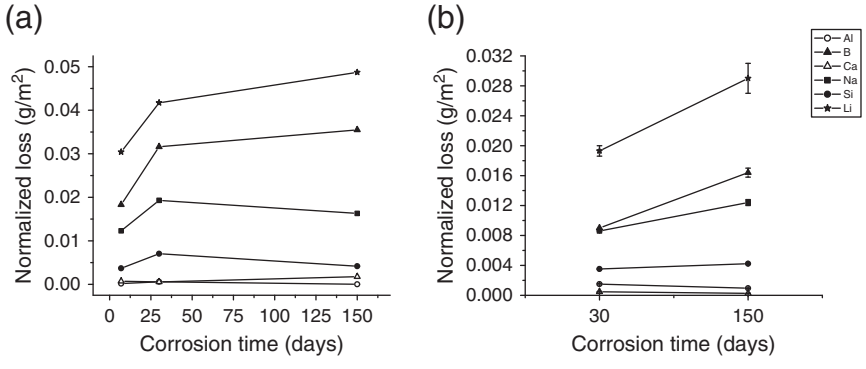

Fig. 2. Normalized loss data for (a) SA1R and (b) AFCI glasses. Error bars for the AFCI measurements represent triplicate solution samples. Please note the variation in the y-axes.

data in this study prevents absolute assignment of the corrosion step for the AFCI samples, but both the one- and five-month samples have not likely reached the residual rate regime. Since SA1R underwent a more rigorous removal of fines, the normalized loss values are higher and the increase in solute concentration was higher. The relative behavior of the components is similar for both glasses. They both rapidly lose lithium with boron and sodium being released more slowly, but still faster than silicon, calcium, and aluminum. The high loss of Li relative to other mobile components has been observed by other corrosion tests on AFCI and other glasses at short times [34]. Calcium, silicon, and aluminum are likely retained in one of the alteration layers.

3.2. ^{29}Si MAS NMR and ^{1}H–^{29}Si CP-CPMG MAS NMR

Based on the results of ^{29}Si MAS NMR Bloch decay experiments, the glass networks of both SA1R (Fig. 3a) and AFCI (Fig. 3b) are comprised of quaternary (Q) $^{[IV]}$Si units, as expected. These data show no discernible differences, indicating that the bulk silicon structure (i.e. pristine portion of the glass) is not affected by the composition, particle size, or exposure time for SA1R and AFCI compositions. More specific Q-site speciation and quantification cannot be accomplished for these samples as next-nearest neighbor Al and B cause an overlapping of the Si–Al and Si–B chemical shift ranges [35,36].

The ^{1}H-containing alteration layers of SA1R, probed using ^{1}H–^{29}Si CP-CPMG MAS NMR, have one distinct resonance similar to that of the pristine glass (Fig. 4a). This broad peak represents multiple indistinguishable resonances due to the heterogeneity of ^{29}Si surface site speciation. The range of Si species contained within this resonance, as well as its lack of resolution into individual Q^n components, is due to the presence of Al as next-nearest neighbor in the alteration layers (Section 3.3). Although these data from SA1R show no evidence of changes to the silicon chemical structure as a function of time, there is a slight increase in the signal-to-noise ratio. As suggested by the normalized loss data (Fig. 2), the loss of mobile species from SA1R is still increasing. Therefore, SA1R has likely not reached the residual rate regime, but this assignment is limited by the lack of kinetic data on this composition. The signal increase may be due to the continued hydration of silica structures with increased time in solution. Moreover, this signal is likely derived from both the hydrated glass and gel layers since silicon should be present and in proximity to ^{1}H in both regions.

After one month of corrosion, the spectrum from the AFCI samples has one definitive silicon environment that is a broad $^{[IV]}$Si resonance similar to that of the pristine glass and SA1R samples (Fig. 4b). There is an indication that a second narrower resonance is present at approximately −92 ppm, at a reduced intensity. As with SA1R, the former is present throughout the alteration layers and increases in intensity with exposure time. The identity of the sharp, crystalline phase could not be determined by X-ray diffraction (XRD) due to the overwhelming signal from the amorphous structure. Crystalline Si phases such as analcime and phyllosilicates have been identified on altered glass surfaces of other nuclear waste glasses corroded for extended times [19,20]. Since AFCI is approaching the residual rate regime, the crystalline phase is likely either a precipitated species at the gel–water interface or phase formed from restructuring of the glass matrix that may eventually lead to alteration renewal at longer corrosion times. After five months of corrosion, no crystalline precursor is detected. The lack of crystalline phases in the five-month sample suggests that secondary phases may precipitate sparingly before the residual rate regime for this sample composition and surface area to volume ratio, but this process is limited by the solution concentrations. No crystalline phase is detected via ^{29}Si NMR for the SA1R glass sample under the same conditions, which indicates that either the low solution concentrations or absence of nucleating agents prevented precipitation (see Fig. 2).

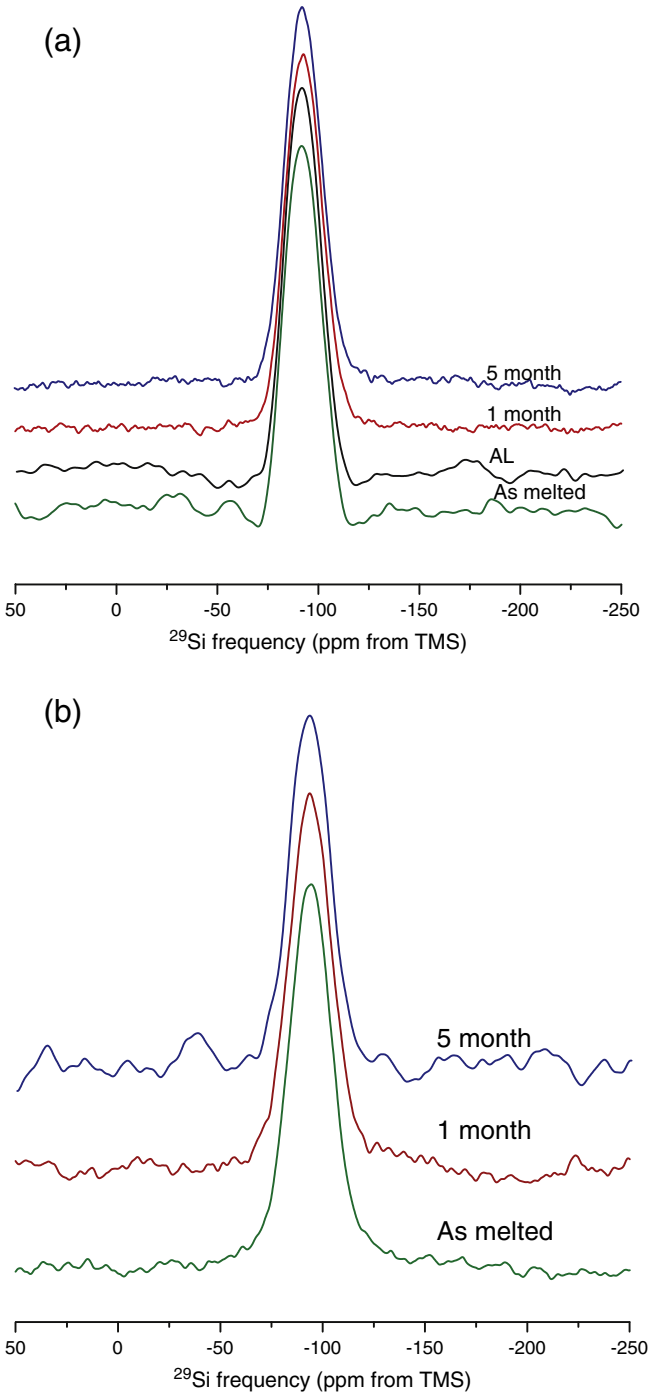

Fig. 3. ^{29}Si MAS NMR spectra of (a) SA1R and (b) AFCI glasses.

3.3. ^{27}Al MAS NMR and ^{1}H–^{27}Al CP-MAS NMR

Al has primarily tetrahedral coordination in the bulk of both glasses as measured by Bloch decay ^{27}Al MAS NMR (Fig. 5). This is the preferential form of aluminum, provided enough network modifying cations are present for charge compensation [37]. In glasses with high aluminum content, such as SA1R and AFCI, aluminum can also adopt octahedral coordination. $^{[VI]}$Al is detected via a resonance at 0 ppm. These two coordination environments are present in the glasses throughout five months of corrosion. There is little change in the ratio of $^{[IV]}$Al to $^{[VI]}$Al with increased corrosion time since a majority of the signal is still derived from the pristine glass.

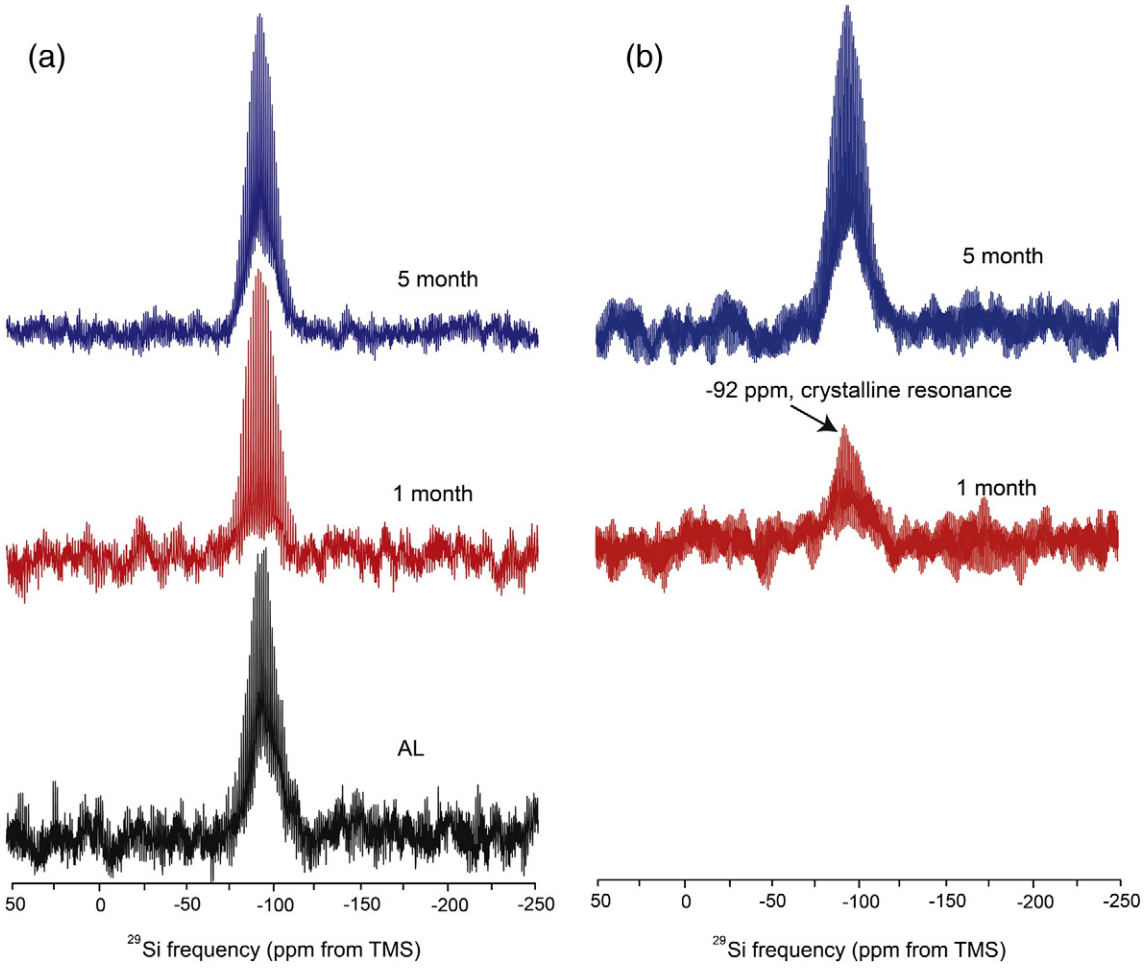

Fig. 4. ^{1}H–^{29}Si CP-CPMG MAS NMR spectra of (a) SA1R and (b) AFCI glasses. The arrow denotes the weak crystalline peak in the AFCI sample corroded for one month.

^{1}H–^{27}Al CP-MAS measurements of alteration layer Al coordination for SA1R provide an interesting insight into the kinetics of layer formation. At shorter exposure periods of one week, $^{[IV]}Al$ is the predominant coordination environment in the alteration layers (Fig. 6a). As the exposure time increases, however, the relative presence of $^{[VI]}Al$ increases. Since cross polarization is not quantitative, the exact ratio of $^{[IV]}Al$ to $^{[VI]}Al$ cannot be determined. These data suggest that the majority of $^{[VI]}Al$ is found in the gel layer and increases as a function of time. The detection of $^{[VI]}Al$ in alteration layers is consistent with previous work by Tsomaia et al. [22]. The presence of $^{[VI]}Al$ is likely a consequence of gel layer formation, where $^{[IV]}Al$ from the hydrated glass layer increases coordination during restructuring. Moreover, the loss of alkali cations with longer corrosion time supports this hypothesis since $^{[VI]}Al$ does not require charge compensation. Furthermore, the asymmetry of the resonance exhibited in the spectrum from the one week basic corroded sample (denoted AL) is indicative of an additional resonance at approximately 30 ppm, representative of $^{[V]}Al$ species. $^{[V]}Al$ is also observed in the one- and five-month exposure samples at ~15 ppm, albeit with a weaker intensity relative to the AL sample. This species may act as an intermediary in the transition between hydrated glass layer $^{[IV]}Al$ to $^{[VI]}Al$ in the gel [38]. This hypothesis is supported by work on mineralic systems, where the dehydroxylation of kaolin to form metakaolin occurs through an unstable $^{[V]}Al$ species [39]. The transition from $^{[IV]}Al$ to $^{[VI]}Al$ through $^{[V]}Al$ may be an indication of Ostwald ripening, where an unstable intermediary is formed when it has an energy close to the starting phase [40]. Jantzen et al. also proposed the mechanism of Ostwald ripening in the formation of alteration layers in other glass systems [41].

The alteration layers of AFCI contain both $^{[IV]}Al$ and $^{[VI]}Al$ (Fig. 6b). The relative amount of $^{[VI]}Al$ is similar for both corrosion periods. Since the loss of mobile species begins to drop before the residual rate regime (Fig. 2), the magnitude of the charge imbalance that promoted coordination change has decreased. Hence, the amount of $^{[VI]}Al$ is essentially constant between one and five months. It should also be noted that aluminum in the crystalline/ordered phase detected via ^{1}H–^{29}Si CP-CPMG is not observed within the limits of observing weak peaks within stronger ones. Therefore, aluminum may be present in this secondary phase, but cannot be observed in this spectrum. As with the SA1R samples, the five-month exposed sample has a feature around 15 ppm, which is also indicative of $^{[V]}Al$.

Criscenti et al. [38] hypothesized that the $^{[VI]}Al$ in the gel layer could be derived from an increase in coordination of $^{[IV]}Al$ in simple glass compositions. The detection of $^{[V]}Al$ prior to $^{[VI]}Al$ formation in the initial rate regime supports this hypothesis and indicates that aluminum coordination increase is one consequence of corrosion/alteration layer formation. Furthermore, very little aluminum was detected in solution by ICP-AES for either AFCI or SA1R. Therefore, the low normalized loss values for aluminum suggest incorporation into the gel layer. We theorize that the hydrous layer structure is comprised of aluminum and silicon with a similar structure to that in the pristine glass. However, the bonding and structural arrangements in the gel are much different since aluminum coordination has increased. These bonding variations are most important for characterizing the transport properties of the altered glass layer.

3.4. ^{11}B MAS NMR and ^{1}H–^{11}B CP-MAS NMR

Boron is a highly soluble species and is often used as a tracer to measure the extent of glass dissolution [1,6,10,16,42–45]. It acts as a

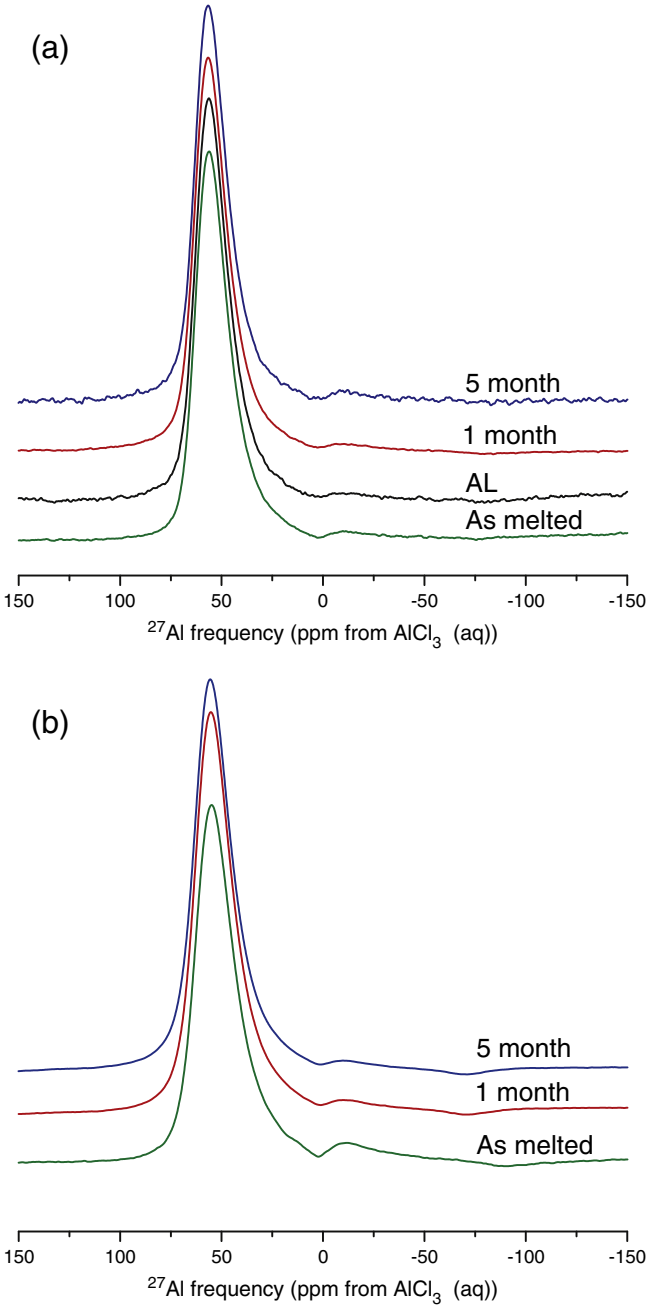

Fig. 5. ^{27}Al MAS NMR spectra of (a) SA1R and (b) AFCI glasses.

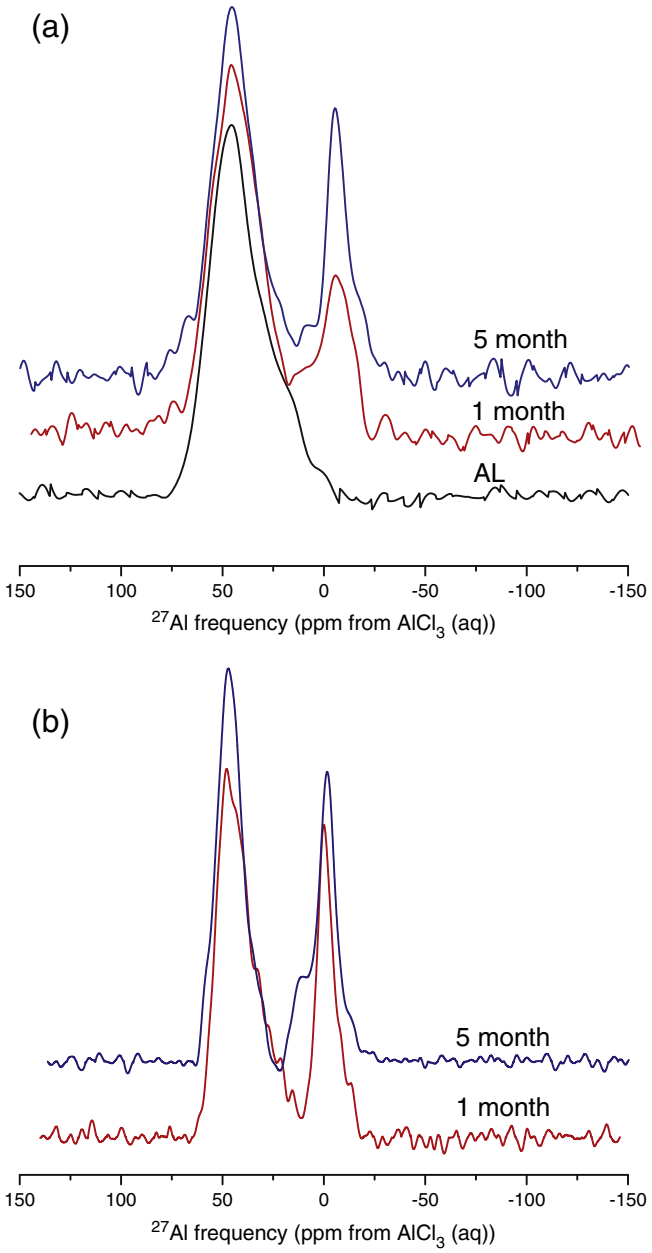

Fig. 6. ^{1}H–^{27}Al CP-MAS NMR spectra of (a) SA1R and (b) AFCI glasses.

network forming species and adopts two coordination environments in the pristine glass: trigonal (~18.0 ppm) and tetrahedral (~2.8 ppm) (Fig. 7). $^{[III]}$B is a stable form in the glass, but the large amount of network modifying cations facilitates an increase in coordination. The conversion to $^{[IV]}$B is coupled with the development of a negative charge on the [BO_4] unit, which must be compensated by the network modifying cations; this is analogous to the local structure of aluminum in silicates. ^{11}B MAS NMR of SA1R indicates that the $^{[III]}$B/$^{[IV]}$B ratio for all time periods is the same within the standard deviation of the data (Table 3, Fig. 7a). This lack of change implies that 1) the degree of corrosion is small, which is supported by the low normalized loss values for boron in SA1R (Fig. 2) and 2) the losses of $^{[III]}$B and $^{[IV]}$B are congruent. Unlike SA1R, AFCI has a slight decrease in the $^{[III]}$B/$^{[IV]}$B ratio between the non-reacted and corroded samples (Fig. 7b, Table 3). The relative amount of $^{[IV]}$B, however, is about the same whether the exposure period was one or five months. We could not determine whether this effect was due to the difference in composition or the presence of fine particles.

CP-MAS NMR data suggest that both $^{[III]}$B and $^{[IV]}$B forms are present in the alteration layers of SA1R (Fig. 8a) and AFCI (Fig. 8b). We posit that this signal is almost exclusively from boron in the hydrated glass layer since other studies have observed boron in the hydrated glass layer, but not in the gel layer [4,14,15]. While previous results are from secondary ion mass spectrometry (SIMS) data for other simulated waste glasses (e.g. SON68), it is reasonable to assume that the boron will also be absent from the layer on AFCI because it is highly mobile. Moreover, the test duration has little influence on the relative amount of $^{[III]}$B and $^{[IV]}$B in the alteration layers for either SA1R or AFCI. If boron were incorporated into the cation-depleted gel layer, there would be an increase in the neutral boron species with corrosion time (as observed for aluminum). The lack of change in the $^{[III]}$B/$^{[IV]}$B

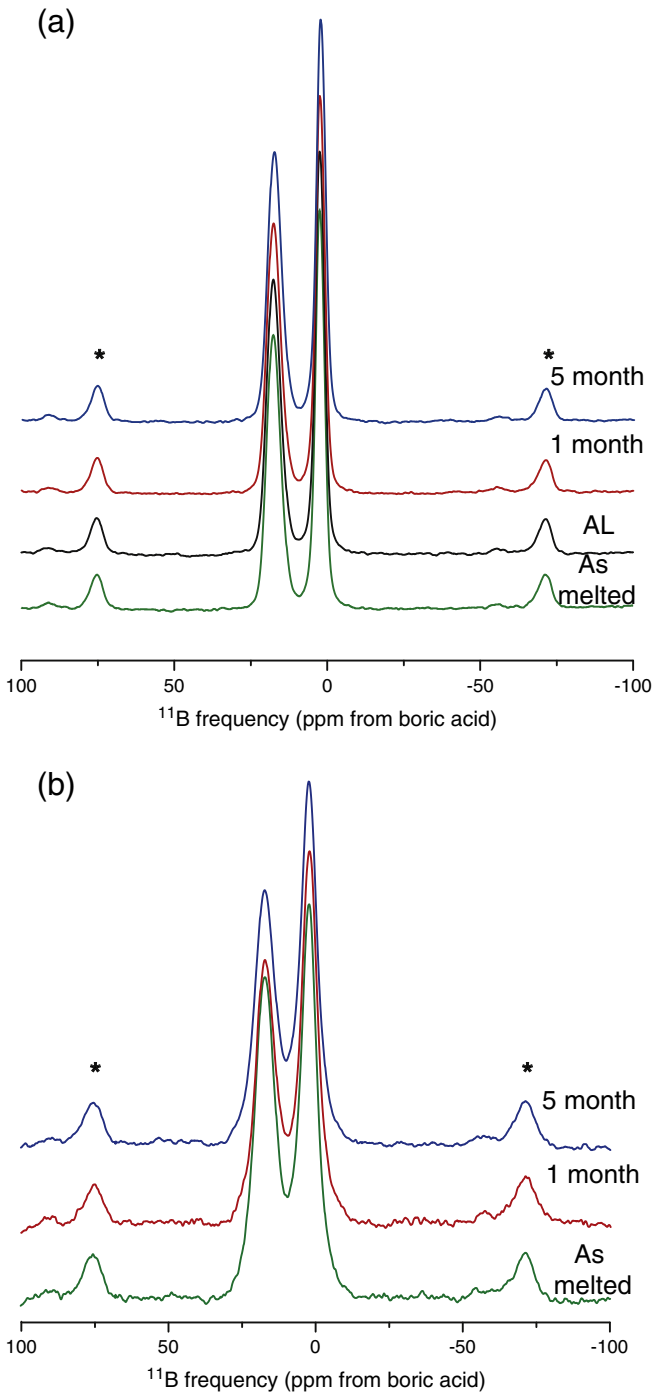

Fig. 7. ^{11}B MAS NMR spectra of (a) SA1R and (b) AFCI glasses. Asterisks denote spinning side bands.

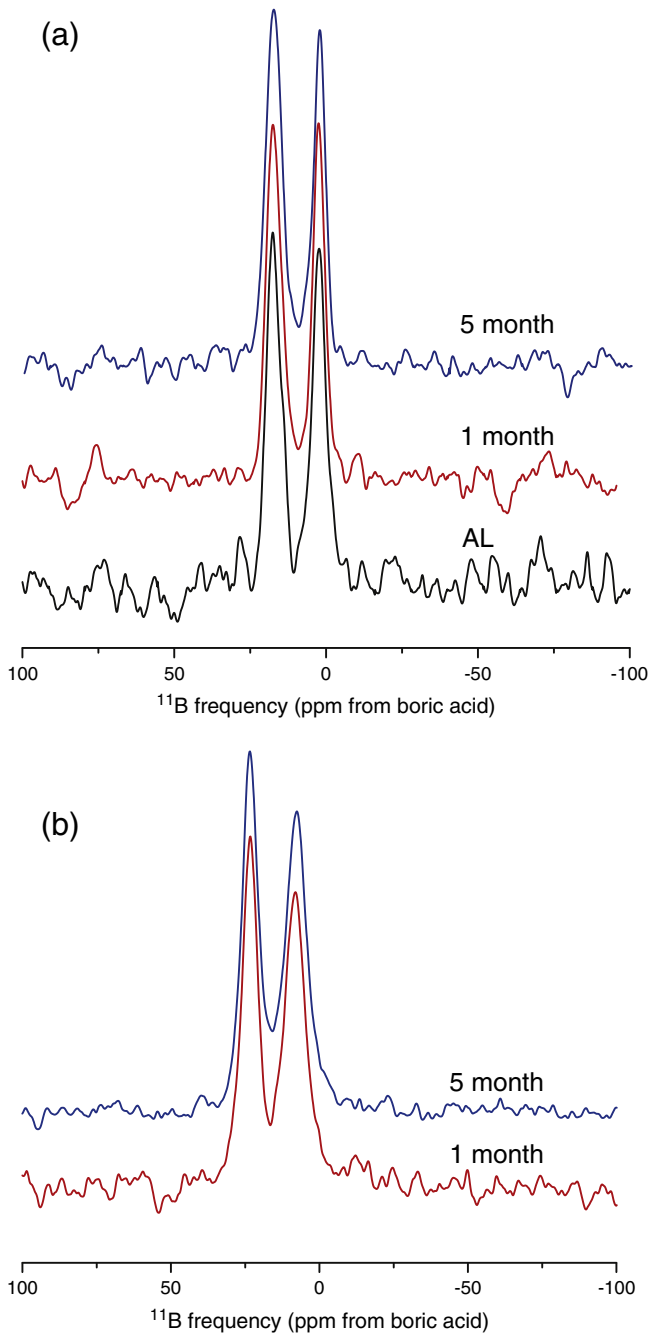

Fig. 8. ^{1}H–^{11}B CP-MAS NMR spectra of (a) SA1R and (b) AFCI glasses. Asterisks denote spinning sidebands.

indicates that boron is likely present within the hydrated glass layer. High-resolution composition analysis of the interface between the gel and hydrated glass layers would help confirm this assignment.

Table 3
$^{[III]}$B/$^{[IV]}$B ratios for AFCI and SA1R as determined by ^{11}B MAS NMR. Peak fitting was completed using NUTS NMR processing software (Acorn Inc.).

Sample	SA1R $^{[III]}$B/$^{[IV]}$B ratio	AFCI $^{[III]}$B/$^{[IV]}$B ratio
As melted	0.92	0.93
1 month in solution	1.0	0.76
5 months in solution	0.91	0.78

3.5. *^{23}Na MAS NMR and ^{1}H–^{23}Na CP-MAS NMR*

Sodium provides charge compensation in the network for negatively charged species such as dangling O bonds, $^{[IV]}$B, and $^{[IV]}$Al (the dominant form of Al in the glass). Therefore, the broad featureless ^{23}Na resonance observed for the pristine SA1R and AFCI glasses is representative of many environments with different numbers of coordinating oxygens (Fig. 9). In SA1R, this environment does not change significantly with increased corrosion time (Fig. 9a). After one month of exposure for the AFCI glass, a second narrow peak also developed that is attributed to a crystalline phase (Fig. 9b). Previous work has observed crystalline metasilicate products with similar chemical shifts of ~21.6 ppm [46]. The crystalline peak observed in the silicon data supports this reaction product identification. After five months of corrosion, a peak

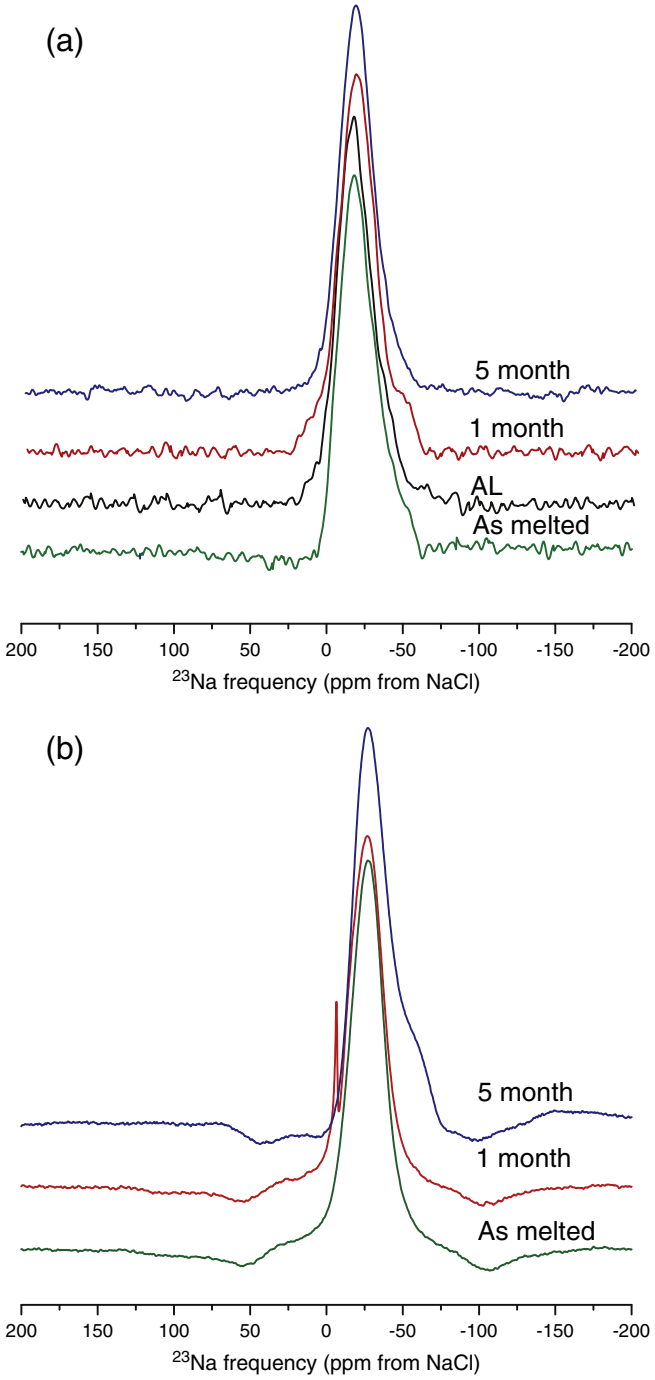

Fig. 9. ^{23}Na MAS NMR spectra of (a) SA1R and (b) AFCI glasses.

from crystalline species is absent. A new, broad resonance appears at a higher frequency relative to the charge-compensating sodium (around −65 ppm). Jones et al. [46] called this region the "quadrupolar tail", which incorporates contributions from sodium-containing silicates and carbonates. The detection of these secondary phases supports the previous assertion that precursors of precipitated phases (either *in situ* or at the gel–water interface) have begun to form at this stage of corrosion and at higher concentrations could possibly lead to alteration renewal.

SA1R and AFCI have weak CP-MAS signals from a lack of Na or proximal ^{1}H in the alteration layers (Fig. 10). Although depleted, sodium is present in the hydrated glass layer where it is required to balance charge-containing species such as $^{[IV]}$Al and $^{[IV]}$B, which are still present. The sodium contained within the hydrated layer likely has a similar environment to that of the sodium in the pristine glass as evidenced by a lack of frequency shift. The sodium resonance corresponds to a non-crystalline silicate as would be expected in the network [47]. The structure of the secondary phase(s) observed in AFCI does not appear to have ^{1}H in close proximity to ^{23}Na because a crystalline species was not detected by CP-MAS. Furthermore, the sodium environment in the hydrated glass layer does not appear to change as a function of time.

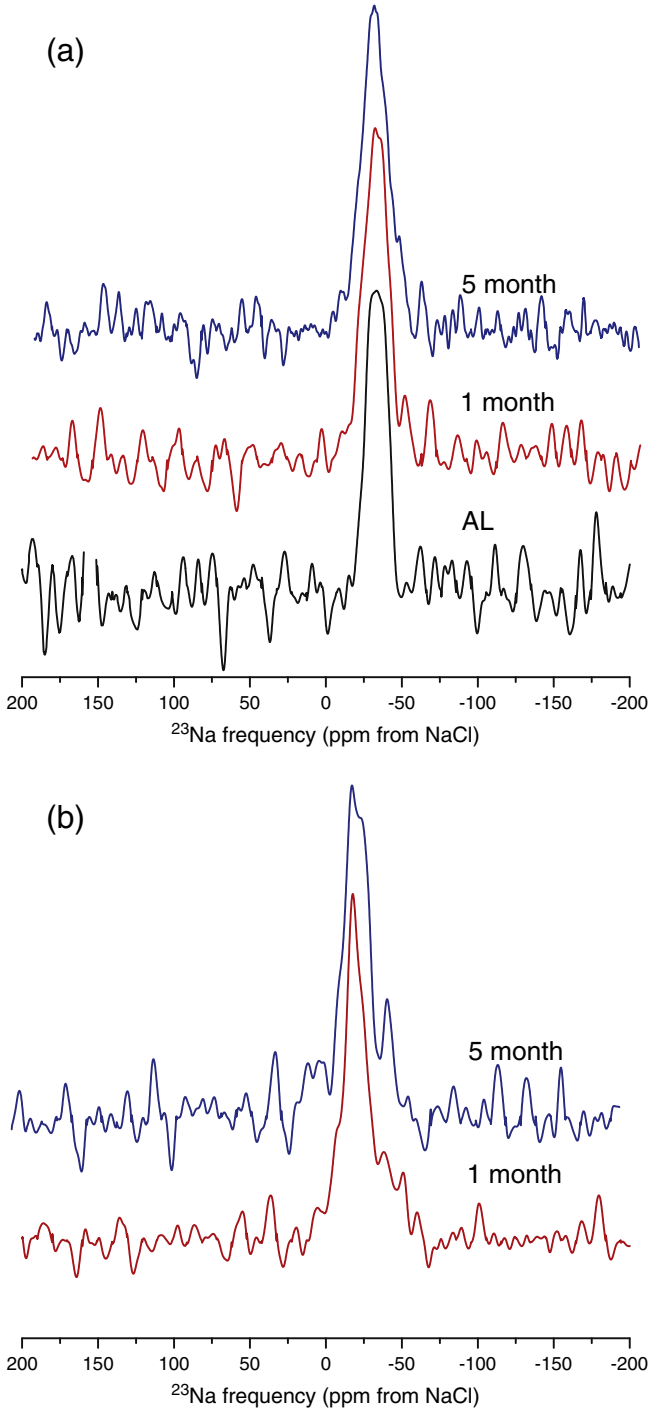

Fig. 10. ^{1}H–^{23}Na CP-MAS NMR spectra of (a) SA1R and (b) AFCI glasses.

3.6. General discussion

The alteration layers appear to be comprised of generally gel and hydrated glass layers, where the latter is found at the interface of the pristine glass and the gel layer. Aluminum from the hydrated glass layer increases in coordination from $^{[IV]}$Al to $^{[VI]}$Al through a $^{[V]}$Al intermediate and is retained in the gel. The lack of aluminum in solution supports this conclusion. In general, the alteration layers appear to have similar silicon environments to those in the pristine glass. Furthermore, silicon is likely contained in both the gel and hydrated glass layer. Sodium and boron are also present in the hydrated glass layer (but not in the gel layer) for both glass compositions. This work is unique in the separate investigation of the structure of the hydrated glass layer relative to the bulk and gel materials.

In general, the structures of the alteration layers and relative trends in component release are similar for AFCI and SA1R glasses. For example, sodium and boron were released at roughly the same rate while significantly more lithium (and less silicon, aluminum, and calcium) was released over the same time period. There are variations, however, that provide interesting insights into the alteration of glasses and suggest that important effects may be overlooked in simplified compositions. The more complex composition of the AFCI glass forms precursor secondary phases such as sodium-containing silicates. These phases either precipitate from solution and adsorb to the gel layer or form from the restructuring in the gel layer. There is support for the latter argument based on ^{1}H–^{27}Al CP-MAS NMR data. The increase in aluminum coordination through an unstable intermediate may suggest Ostwald ripening, which could also explain secondary phase formation since a mineral is more stable than the gel phase [41].

Variations in the ^{1}H–^{29}Si CP-CPMG MAS NMR signals for both samples indicate that the alteration layers continue to hydrate over time. These changes are related to the dynamics between the alteration layers and solution phase Si. This implies that the pristine glass acts as the initial source of Si in the alteration layers, while recondensation reactions become important in the gel layer formation at higher Si solution concentrations. Future work will focus on addressing this question. There were no ^{1}H–^{27}Al CP-MAS NMR signal changes between the one- and five-month corroded AFCI samples, suggesting that for aluminum at least, the structure in the gel is more stable.

Based on this work, hypotheses can be posited regarding the viability and stability of a glass matrix for disposal of radioactive waste. Retention of glass components appears to be a function of incorporation in the gel layer, facilitated by an increase in coordination for aluminum. This suggests that the compatibility of the coordination environment of the radioactive component with the gel layer structure or the potential to change that environment may influence the retention. Radioactive components will likely be present in the hydrated glass layer since we observed mobile species (B and Na) here. Previous work has posited that there is a diffusion barrier for some species, which controls the potential loss to solution [25]. Therefore, the reaction dynamics in this layer must be evaluated since it will have a significant impact on the retention of radioactive components. Finally, secondary phases have been observed to form prior to the residual rate regime. Since precipitation of these phases may lead to corrosion resumption, the AFCI composition may not be optimal for long-term waste storage.

4. Conclusions

The environments of several recondensation nuclei in the alteration layers of the two glasses have been studied by solid-state NMR spectroscopy. A robust characterization of the structures of the alteration layers is essential to evaluate their roles in the mechanisms that lead to the residual rate regime for glass dissolution. The transfer of polarization from ^{1}H nuclei, which are only found in the hydrous layer, to another component in CP-MAS NMR experiments allowed comparisons to be made between the altered surface and pristine glass structures. In this study, we successfully identified the hydrated layer, a barrier between the pristine glass and gel layer. We determined that this layer acts as an intermediary zone in which glass components are either incorporated into the gel layer or lost to solution. Furthermore, we found that simplified glass compositions provide general trends in the formation of alteration layers, but do not account for precursor secondary phases that form before reaching the residual rate regime.

Based on the structural characterization of the alteration layers produced during the corrosion of glass in a static solution, hypotheses about the formation of the gel layer and hydrated glass layer can be inferred. The hydrated glass layer is an intermediate between the gel layer and pristine glass and maintains the structure of insoluble components before they eventually restructure into the gel layer. Since the hydrated glass layer influences the growth of the gel, both layers must be considered in the kinetics of nuclear waste glass corrosion; although, other factors are likely involved. It may be that other mechanisms control corrosion in addition to those found within the affinity and protective barrier models. Restructuring to form the gel layer, however, appears to be a function of component solubility and stability.

Acknowledgments

This work was funded by the Nuclear Energy University Program (NEUP) under contract number 00101956. We would like to acknowledge the EMSL NMR user facility at PNNL and its personnel, especially Jinfeng Lai and Sarah Burton, for their assistance in data collection. A portion of this research was performed using EMSL, a national scientific user facility sponsored by the Department of Energy's Office of Biological and Environmental Research and located at Pacific Northwest National Laboratory. We would also like to thank Henry Gong for ICP-AES measurements and Julie Anderson for BET measurements.

References

[1] P. Van Iseghem, M. Aertsens, S. Gin, D. Deneele, B. Grambow, P. McGrail, D. Strachan, G. Wicks, GLAMOR: A Critical Evaluation of the Dissolution Mechanisms of High Level Waste Glasses in Conditions of Relevance for Geological Disposal, in, 2007, , 2007.
[2] B. Bergeron, L. Galoisy, P. Jollivet, F. Angeli, T. Charpentier, G. Calas, S. Gin, J. Non-Cryst. Solids 356 (2010) 2315–2322.
[3] C. Cailleteau, F. Angeli, F. Devreux, S. Gin, J. Jestin, P. Jollivet, O. Spalla, Nat. Mater. 7 (2008) 978–983.
[4] S. Gin, C. Guittonneau, N. Godon, D. Neff, D. Rebiscoul, M. Cabie, S. Mostefaoui, J. Phys. Chem. C 115 (2011) 18696–18706.
[5] D. Rebiscoul, F. Rieutord, F. Ne, P. Frugier, R. Cubitt, S. Gin, J. Non-Cryst. Solids 353 (2007) 2221–2230.
[6] E.M. Pierce, E.A. Rodriguez, L.J. Calligan, W.J. Shaw, B.P. McGrail, Appl. Geochem. 23 (2008) 2559–2573.
[7] D.M. Strachan, T.L. Croak, J. Non-Cryst. Solids 272 (2000) 22–33.
[8] J. Neeway, A. Abdelouas, B. Grambow, S. Schumacher, J. Nucl. Mater. 415 (2011) 31–37.
[9] K. Ferrand, A. Abdelouas, B. Grambow, J. Nucl. Mater. 355 (2006) 54–67.
[10] B. Grambow, R. Muller, J. Nucl. Mater. 298 (2001) 112–124.
[11] S. Gin, C. Jegou, P. Frugier, Y. Minet, Chem. Geol. 255 (2008) 14–24.
[12] P. Aagaard, H.C. Helgeson, Am. J. Sci. 282 (1982) 237–285.
[13] E.H. Oelkers, Geochim. Cosmochim. Acta 65 (2001) 3703–3719.
[14] A.R. Lodding, E.U. Engstrom, B.K. Zoitos, D.E. Clark, G.G. Wicks, J. Am. Ceram. Soc. 75 (1992) 2702–2706.
[15] A. Lodding, P. Van Iseghem, J. Nucl. Mater. 298 (2001) 197–202.
[16] E. Curti, J.L. Crovisier, G. Morvan, A.M. Karpoff, Appl. Geochem. 21 (2006) 1152–1168.
[17] W.L. Gong, L.M. Wang, R.C. Ewing, E. Vernaz, J.K. Bates, W.L. Ebert, J. Nucl. Mater. 254 (1998) 249–265.
[18] E. Pelegrin, G. Calas, P. Ildefonse, P. Jollivet, L. Galoisy, J. Non-Cryst. Solids 356 (2010) 2497–2508.
[19] S. Ribet, S. Gin, J. Nucl. Mater. 324 (2004) 152–164.
[20] N. Valle, A. Verney-Carron, J. Sterpenich, G. Libourel, E. Deloule, P. Jollivet, Geochim. Cosmochim. Acta 74 (2010) 3412–3431.
[21] J.P. Hamilton, C.G. Pantano, J. Non-Cryst. Solids 222 (1997) 167–174.
[22] N. Tsomaia, S.L. Brantley, J.P. Hamilton, C.G. Pantano, K.T. Mueller, Am. Mineral. 88 (2003) 54–67.

[23] R. Conradt, J. Am. Ceram. Soc. 91 (2008) 728–735.
[24] F. Angeli, M. Gaillard, P. Jollivet, T. Charpentier, Geochim. Cosmochim. Acta 70 (2006) 2577–2590.
[25] P. Frugier, S. Gin, Y. Minet, T. Chave, B. Bonin, N. Godon, J.E. Lartigue, P. Jollivet, A. Ayral, L. De Windt, G. Santarini, J. Nucl. Mater. 380 (2008) 8–21.
[26] E. Curti, R. Dahn, F. Farges, M. Vespa, Geochim. Cosmochim. Acta 73 (2009) 2283–2298.
[27] P. Jollivet, F. Angeli, C. Cailleteau, F. Devreux, P. Frugier, S. Gin, J. Non-Cryst. Solids 354 (2008) 4952–4958.
[28] C. Cailleteau, F. Devreux, O. Spalla, F. Angeli, S. Gin, J. Phys. Chem. C 115 (2011) 5846–5855.
[29] F. Angeli, T. Charpentier, M. Gaillard, P. Jollivet, J. Non-Cryst. Solids 354 (2008) 3713–3722.
[30] F. Angeli, O. Villain, S. Schuller, S. Ispas, T. Charpentier, Geochim. Cosmochim. Acta 75 (2011) 2453–2469.
[31] C. Poinssot, S. Gin, J. Nucl. Mater. 420 (2012) 182–192.
[32] J.V. Crum, A.L. Billings, J. Lang, J.C. Marra, C. Rodriguez, J.V. Ryan, J.D. Vienna, Baseline Glass Development for Combined Fission Products Waste Streams, AFCI-WAST-WAST-MI-DV-2009-000075, Pacific Northwest National Laboratory, Richland, WA, 2009.
[33] ASTM Standard C 1285-02 Standard Test Methods for Determining Chemical Durability of Nuclear, Hazardous, and Mixed Waste Glasses and Multiphase Glass Ceramics: The Product Consistency Test (PCT), ASTM International, West Conshohocken, PA, 2002.
[34] W.L. Ebert, J.A. Fortner, A.L. Billings, C. Crawford, Glass Testing Activities at ANL and SRNL: FY11, *Progress Report*, FCRD-WAST-2011-000404, Fuel Cycle Research and Development Program, 2011.
[35] T. Nanba, M. Nishimura, Y. Miura, Geochim. Cosmochim. Acta 68 (2004) 5103–5111.
[36] C.A. Fyfe, Y. Feng, H. Grondey, G.T. Kokotailo, H. Gies, Chem. Rev. 91 (1991) 1525–1543.
[37] A. Varshneya, Fundamentals of Inorganic Glasses, Academic Press, Boston, 1994.
[38] L.J. Criscenti, S.L. Brantley, K.T. Mueller, N. Tsomaia, J.D. Kubicki, Geochim. Cosmochim. Acta 69 (2005) 2205–2220.
[39] S. Sperinck, P. Raiteri, N. Marks, K. Wright, J. Mater. Chem. 21 (2011) 2118–2125.
[40] W. Ostwald, Z. Phys. Chem. 22 (1897) 289–330.
[41] C.M. Jantzen, K.G. Brown, J.B. Pickett, Int. J. Appl. Glas. Sci. 1 (2010) 38–62.
[42] T. Chave, P. Frugier, A. Ayral, S. Gin, J. Nucl. Mater. 362 (2007) 466–473.
[43] C. Martin, I. Ribet, P. Frugier, S. Gin, J. Nucl. Mater. 366 (2007) 277–287.
[44] P. Vaniseghem, T. Amaya, Y. Suzuki, H. Yamamoto, J. Nucl. Mater. 190 (1992) 269–276.
[45] E. Vernaz, S. Gin, C. Jegou, I. Ribet, J. Nucl. Mater. 298 (2001) 27–36.
[46] A.R. Jones, R. Winter, P. Florian, D. Massiot, J. Phys. Chem. B 109 (2005) 4324–4332.
[47] J.M. Egan, K.T. Mueller, J. Phys Chem. B 104 (2000) 9580–9586.